Materials Science in Semiconductor Processing 35 (2015) 59–65

Contents lists available at ScienceDirect

Materials Science in Semiconductor Processing

journal homepage: www.elsevier.com/locate/mssp

Enhancing power conversion efficiency of DSSC by doping SiO_2 in TiO_2 photo anodes

K. Balachandran [a,*], Rajendran Venckatesh [b], Rajeshwari Sivaraj [c], K.V. Hemalatha [d], R. Mariappan [e]

[a] Department of Chemistry, Vivekanandha College of Engineering for women, Namakkal, Tamil Nadu, India
[b] Department of Chemistry, Government Arts College, Udumalpet 642126, Tamil Nadu, India
[c] Department of Biotechnology, School of Life Sciences, Karpagam University, Eachanari Post, Coimbatore 641021, Tamil Nadu, India
[d] Department of Chemistry, Coimbatore Institute of Technology, Coimbatore, Tamil Nadu, India
[e] Department of Physics, Adhiyaman College of Engineering, Hosur, Tamil Nadu, India

ARTICLE INFO

Available online 19 March 2015

Keywords:
Nanocomposites
eosin-Y
Blueshift
Quantum confinement effect
Surface area

ABSTRACT

A simple, less time consuming, cost ineffective sol–gel method was used to synthesis TiO_2 nanoparticles (TiO_2) and TiO_2–SiO_2 nanocomposites (TiO_2–SiO_2) using titanium tetra isopropoxide as TiO_2 and silicic acid as SiO_2 precursors respectively. The synthesized nanocomposites were characterized by XRD, SEM, TEM, UV–visible, FTIR and BET analysis. The quantum confinement effect of TiO_2 and TiO_2–SiO_2 was confirmed by a blueshift observed in UV–visible spectra. The band observed at 950 cm^{-1} in FTIR analysis confirmed the presence of Ti–O–Si bonds, the TEM analysis shows both the TiO_2 and TiO_2–SiO_2 were in nanometer size. The BET (Brunauer– Emmett–Teller) specific surface areas of the samples were 65 and 75 m^2/g for TiO_2 and TiO_2–SiO_2 respectively. The power conversion efficiency (PCE) of the nanocomposites were studied by using Keithely electrometer and multimeter and it was found to be 2% and 2.5% for eosin-Y sensitized TiO_2 and TiO_2–SiO_2 nanocomposites respectively.

© 2015 Elsevier Ltd. All rights reserved.

1. Introduction

Due to population explosion and industrialization power (electricity) demand increases day by day. In order to relieve the energy crises, environment pollution and global warming the development of accessible renewable energy production has received substantial attention. Solar power is the most noteworthy among renewable and sustainable energy resources. In recent years dye sensitized solar cells (DSSC) gained much attention because of its properties such as low fabrication cost, robust nature, environmental compatibility and simplicity of the process [1–3].

Recently, nanosized TiO_2 powders have been used as a working electrode for dye sensitized solar cells due to its higher efficiency than any other metal oxide semiconductor. However as reported the best TiO_2 solar efficiency could hardly reach 11.5% [4]. Additionally TiO_2 has proven to be the most suitable for wide spread solar energy conversion and environmental applications due to its biological, chemical inertness, strong oxidizing power, cost effectiveness, long term stability against photo corrosion and chemical corrosion [5].

The physical and chemical properties of TiO2 size can be modified by adding second semiconductor into the TiO_2 matrix. Silicon dioxide (SiO_2) has been incorporated into the TiO_2 matrix to enhance the photocatalytic process [6–9]. Addition of SiO_2 content can suppress the crystal growth of TiO_2 grains [6,8]. SiO_2 has high thermal stability, excellent

* Corresponding author. Mobile: +91 9865571959.
E-mail address: balanano06@gmail.com (K. Balachandran).

http://dx.doi.org/10.1016/j.mssp.2015.02.071
1369-8001/© 2015 Elsevier Ltd. All rights reserved.

mechanical strength and helps to create new catalytic active sites due to interaction between TiO_2 and SiO_2 [10]. SiO_2 acts as the carrier of TiO_2 and helps to obtain a large surface area as well as suitable porous structure [11].

A number of methods have been applied to fabricate TiO_2–SiO_2 composites, including e-beam evaporation, chemical vapor deposition, flame hydrolysis, spray pyrolysis and sol–gel [12]. The interest in the use of sol–gel methods is due to several advantages: good homogeneity, ease of composition control, low processing temperature, ability to fabricate large area coatings and low equipment cost [12,13].

In DSSC the counter electrode plays a major role to improve the electron transportation. Although Platinum coated FTO as the counter electrode is usual. It is expensive and it could be corroded in tri-iodide containing solutions to generate platinum iodides such as PtI_4 [14,15]. So most of the researchers search alternative counter electrode for corrosion inert and exhibit good catalytic activity for the reduction of tri-iodide ion. As a result many types carbonaceous materials such as carbon nanotubes [16] carbon black [17] and graphite [18] were used as counter electrode.

In the present work we synthesized TiO_2 and TiO_2–SiO_2 nanocomposites by a Sol–gel method and it was characterized by XRD, UV–visible, SEM, TEM, FTIR, EDAX and BET analysis. The photovoltaic performances of eosin-Y sensitized TiO_2 and TiO_2–SiO_2 photo anodes were studied by using carbon coated FTO as counter cathode. The study also reveals that the effect of doping SiO_2 in TiO_2.

2. Materials and methods

2.1. Materials

All reagents used were of analytical grade purity and were procured from Merck Chemical Reagent Co., Ltd., India.

2.2. Synthesis of TiO_2 nanoparticles

Titanium tetra isopropoxide (TTIP) was used as a precursor, Hydrochloric acid (HCl) as peptizing agent and ethanol was used as solvent medium. 2 mL of HCl was mixed with 50 mL of ethanol and was stirred for few minutes. To this mixture 20 mL of TTIP was added and the stirring was continued for 1 h at room temperature. Then 50 ml of distilled water was added, the temperature was raised to 50 °C and stirred for 3 h until the solution changed into colorless gel. The high viscous gel was dried at room temperature to fine powder. The resulting powder was heated at 120 °C for 1 h in a hot air oven to remove the moisture and other solvents. Finally the colorless powder was calcined at 400 °C to increase the crystallinity and to remove the carbonaceous materials present in TTIP.

2.3. Synthesis of TiO_2–SiO_2 nanocomposites

1 M SiO_2 sol was prepared by mixing 0.96 g of silicic acid with 10 mL of THF (Tetrahydrofuran). 10 mL of SiO_2 sol was added drop-wise to the TiO_2 sol, which resulted in yellowish brown solution. The mixture was stirred for 3 h at room temperature, then the temperature was raised to 80 °C and stirring was continued for an hour. Finally yellowish brown changes to yellow and then the solution was dried at room temperature. Yellow powder was obtained and it was heated in hot air oven at about 120 °C for 1 h to remove the moisture and other solvents. Finally the composites were calcined at 400 °C to increase the crystallinity and to remove the carbonaceous materials present in TTIP.

2.4. Characterization of synthesized TiO_2 nanoparticles and TiO_2–SiO_2 nanocomposites

Synthesized TiO_2 nanoparticles and TiO_2–SiO_2 nanocomposites optical properties were characterized by UV–visible spectroscopy (Carry 5000 UV–vis-NIR spectrophotometer, Varian, USA). The crystalline structure of synthesized TiO_2 nanoparticles and TiO_2–SiO_2 nanocomposites were analyzed using a D8 Advance X-ray diffraction meter (Bruker AXS, Germany) at room temperature, operating at 30 kV and 30 mA, using Cu Kα radiation (k=0.15406 nm) and crystal size was calculated by Scherrer's formula. EDAX and Surface morphology of synthesized TiO_2 nanoparticles and TiO_2–SiO_2 nanocomposites were characterized using a scanning electron microscope (SEM) (Model JSM 6390LV, JOEL, USA). The nanoparticles and composites were viewed through transmission electron microscope (TEM) (JEOL-TEM 2100) at high magnification and exact particle size was predicated. TiO_2 nanoparticles and TiO_2–SiO_2 nanocomposites functional groups were described using Fourier Trans-form infrared spectroscopy (FTIR) spectra (Thermo Nicolet, USA) with a wave number range of 4000–400 cm^{-1}. The surface area, pore size and pore volume of the nanocomposites were analyzed using BET analyzer model Micromeritics Gemini 2375, Surface Area Analyzer (Micromeritics Inc., Norcross, GA). The power conversion efficiency (PCE) of the nanocomposites were studied by using Keithely electrometer and multimeter 2450. The results are discussed and reported.

2.5. Fabrication of DSSC

2.5.1. Preparation of TiO_2, TiO_2–SiO_2 electrode and treatment with dye

Thin nano structured photo-anode film was fabricated using synthesized TiO_2 and TiO_2–SiO_2 nanocomposites by employing doctor blade technique. TiO_2 and TiO_2–SiO_2 nanomaterials were ground by a mortar and pestle with addition of appropriate amount of distilled water and methanol. After making a viscous paste, it was further diluted with distilled water and then a few drops of triton X-100 was added for better adhesion of the paste on conducting substrate. The paste was spread on the conducting substrate with a glass rod using adhesive tape as spacers. After drying in air, the film was sintered for 30 min at 400 °C in a muffle furnace. After sintering, the TiO_2 and TiO_2–SiO_2 film was sensitized in 0.5 mM of eosin-Y containing acetonitrile dye solution as for 12 h. The dye-sensitized electrodes were rinsed with acetonitrile to remove excess unanchored dye molecules on the surface. The same procedure was followed for eosin-Y sensitized TiO_2–SiO_2 composites.

2.5.2. Film thickness measurement

The thickness of samples was measured using an Alpha-Step-D-600 Stylus Profiler. Thin nano structured

photo-anode film was fabricated using synthesized TiO_2 and TiO2–SiO_2 nanocomposites by with film thickness as 230 nm for TiO_2 and 253 nm for TiO_2–SiO_2 nanocomposites through employing doctor blade technique.

2.5.3. Preparation of counter electrode

Preparation of counter electrodes followed the method described in [17]. To prepare the carbon counter electrode pastes with five different EG/5B pencil-lead weight ratios of 1:0, 1:1, 1:2, 2:1 and 0:1, 130 mg EG was respectively mixed with different weight 5B pencil-lead according to the weight ratios. To each 130 mg mixture, 0.6 ml TiO_2 colloid, 1.2 ml water, 0.6 ml 10% Triton X-100 aqueous solution, and 1 ml ethanol were added. After milling for an hour, the carbon counter electrode pastes were obtained. It was then coated on the FTO conductive glass using the doctor blade technique. After dried for 30 min at room temperature, the substrate was heated at 450 °C for an hour. So the carbon counter electrode was prepared.

2.5.4. Electrolyte preparation

The electrolyte solution was composed of 0.5 M LiI/0.05 M I/0.5 M TBP (Tetra butyl pyridine), it was prepared by 0.63 g of iodine (Mol. Wt.=126.9), 6.7 g of lithium iodide (LiI) (Mol.Wt.=133.8) and 9.5 g of TBP (Mol.Wt.=191.3) dissolved in 100 mL of acetonitrile solution.

2.5.5. Assembly of TiO_2 based DSSC

DSSC was fabricated using standard two-electrode configurations, comprising dye sensitized TiO_2/FTO (with an active surface area of 0.25 cm^2) as photo anode, carbon coated FTO as a counter electrode. For two-electrode measurement, the liquid electrolyte I^-/I_3^- was injected between photo anode and counter cathode, pressing firmly. A thin layer of para film was used as a spacer to avoid short-circuiting between two electrodes. A binder clip was fixed externally to maintain the mechanical grip of the cell without any further sealing, which finalized the assembly of the DSSC. The *V–I* characteristics of current was measured by Keithley electrometer under the light radiation source of 1000 W/cm^2. The same procedure was followed for TiO_2–SiO_2 composites. The following cell configurations were used to record *I–V* plots:

$$FTO/TiO_2/eosin-Y/I^-/I_3{}^-/C/FTO$$

$$FTO/TiO_2-SiO_2/eosin-Y/I^-/I_3{}^-/C/FTO$$

3. Results and discussion

3.1. Determination of surface area—B.E.T method

The BET specific surface areas of the samples calcined at 400 °C were 65 and 75 m^2/g for TiO_2 and TiO_2–SiO_2, respectively. The characterization of the TiO_2 doped materials has been reported elsewhere. The surface area of the TiO_2–SiO_2 increased as a result of doping SiO_2 in TiO_2. It is possible that the SiO_2 form clusters of nanoparticles within a TiO_2 nanoparticle sphere thereby displacing some of the TiO_2 particles and increasing the surface area. This data strongly suggest that during calcination the TiO_2 and SiO_2 react with one another and increases the surface area of the composites. (Fig. 1)

3.2. Characterizations of TiO_2 nanoparticles and TiO_2–SiO_2 nanocomposites

Fig. 2 represents UV–visible spectra of TiO_2 and TiO_2–SiO_2. It is shown that TiO_2 is an oxide semiconductor and its anatase form has an optical absorbance range around 384 nm, band gap 3.2 eV. In the current measurement the onset of absorption peak of maximum absorbance occurred at 372 nm for TiO_2 and 352 nm for TiO_2–SiO_2 nanocomposites. The blueshift in absorbance corresponds to smaller particle size. The blue shift observed in the absorbance spectra indicated the Quantum confinement effect [19]. The optical band gap of the material was calculated by effective mass approximation and it was found to be 3.3 for TiO_2 and 3.54 for TiO_2–SiO_2 nanocomposites. Increase in the band gap of the prepared composites allowed for possible applications like photo luminescence, photocatalytic and optoelectronic device fabrications. Since the results derived from the study reveal that enhanced band gap could be a better photo catalyst light below its wave length holds sufficient energy

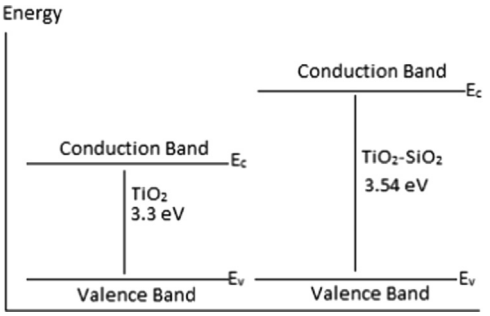


Fig. 1. Energy band diagram of TiO_2 and TiO_2–SiO_2 nanocomposites.

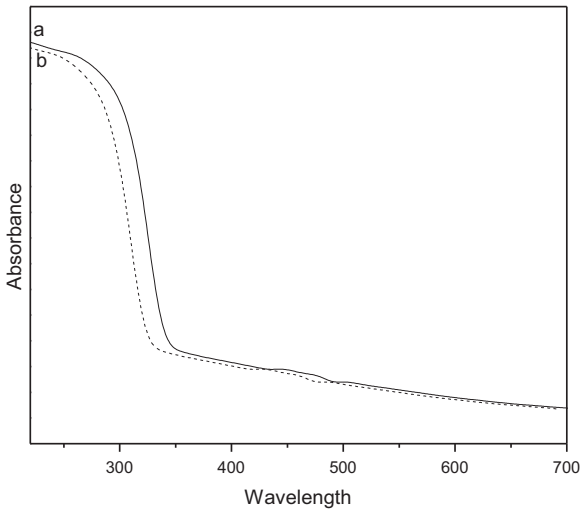


Fig. 2. UV–visible spectra of (a) TiO_2 and (b) TiO_2–SiO_2 nanocomposites.

to excite the electrons and hence absorbed by TiO_2 based composites. Therefore both TiO_2, TiO_2–SiO_2 are excellent UV absorbers [20].

Fig. 3 represents XRD patterns of TiO_2 and TiO_2–SiO_2 nanocomposites. The crystallite types of the TiO_2–SiO_2 nanocomposites were pure anatase. The most intense reflection at $2\theta = 25.3^\circ$ is assigned to anatase (d101). Not much difference has been detected between patterns of TiO_2 and TiO_2–SiO_2. The powders showed the crystalline pattern and the observed d-lines match the reported values for the anatase phase. The intensity of reflections appeared to be increased for TiO_2–SiO_2 as compared to TiO_2 due to inclusion of SiO_2. The average crystallite size was determined by carrying slow scan of the powders in the range 24–27 with the step of 0.01-min^{-1} from Scherrer's equation using the (101) reflections of the anatase phase assuming spherical particles. An estimate of the grain size (G) from the broadening of the main (101) anatase peak can be done by using the Scherrer formula. The nanocrystallite sizes were found to be 15–20 nm for TiO_2 while 7–10 nm for TiO_2–SiO_2 powders. The weakening and broadening of the XRD peaks may be attributed to the decrease of the sample grain size and the increase of the SiO_2 content. The introduction of SiO_2 can effectively suppress the grain growth of anatase compared with pure TiO_2. Moreover, the suppression is more remarkable with the introduction of higher silica content, which is consistent with the literature [21]. The major differences were the narrower first maximum and the broader second maximum.

Fig. 4 represents SEM and TEM images of TiO_2 and TiO_2–SiO_2 nanocomposites. The SEM and TEM images along with the particle size distribution of the pure TiO_2 nanoparticles and TiO_2–SiO_2 nanocomposites. The pure TiO_2 particles exhibited irregular morphology due to the agglomeration of primary particles and with an average diameter of 15–20 nm. On the other hand, TiO_2–SiO_2 nanocomposites exhibited regular morphology. The average particle size of the colloidal TiO_2–SiO_2 nanocomposites was measured to be 7–10 nm.

Fig. 5 represents the FT-IR spectra of TiO_2 particles and TiO_2–SiO_2 composites. The peaks at 3400 and 1650 cm^{-1} in the spectra are due to the stretching and bending vibration of the $-OH$ group. In the spectrum of pure TiO_2, the peaks at 550 cm^{-1} show stretching vibration of Ti–O and peaks at 1450 cm^{-1} show stretching vibrations of Ti–O–Ti. The spectrum of TiO_2–SiO_2 shows the peaks at 1400 cm^{-1}, 450–550 cm^{-1} exhibiting stretching modes of Ti–O–Ti, 1100 cm^{-1} show Si–O–Si bending vibrations and peak at 950 cm^{-1} shows Si–O–Ti vibration modes which is due to the overlapping from vibrations of Si–OH and Si–O–Ti bonds. This result indicates that the TiO_2–SiO_2 nanocomposites were prepared by a combination of TiO_2 with SiO_2 nanoparticles. Fig. 6 shows the EDAX analysis of TiO_2 and TiO_2–SiO_2. The EDAX analysis shows the presence of Ti, Si and O atoms. From the EDAX analysis it was confirmed that 1% silica was present in the composites.

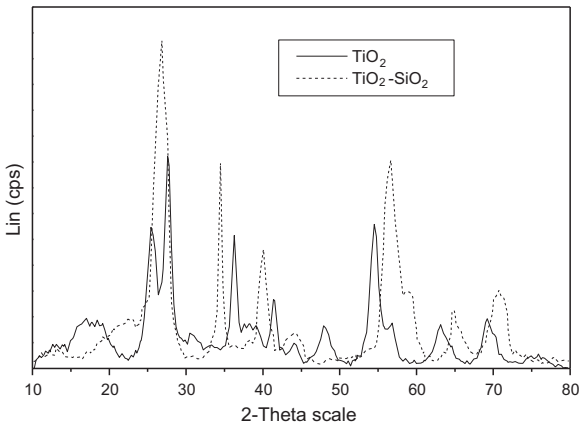


Fig. 3. XRD patterns of TiO_2 and TiO_2–SiO_2 nanocomposites.

3.3. Photovoltaic performances of dye sensitized solar Cells

The current – voltage (I–V) characteristics of DSSC constructed by using TiO_2 particles and TiO_2–SiO_2 composites sensitized with eosin-Y under illumination condition (1000 W cm^{-2}) are shown in Fig. 7 The fill factor and conversion efficiency of the fabricated TiO_2 and TiO_2–SiO_2 based DSSC is calculated as follows

$$FF = \frac{V_{max} * J_{max}}{V_{oc} * J_{sc}}$$

$$\eta = \frac{FF * V_{oc} * J_{sc}}{P_{in}}$$

where

V_{oc} = open circuit voltage, J_{sc} = short circuit current, V_{max} = maximum voltage,

J_{max} = maximum current density, P_{in} = power input (1000 W/cm^2).

The I–V curves of eosin-Y sensitized TiO_2 and TiO_2–SiO_2 were shown in Fig. 7. The short-circuit current density (J_{SC}) were found to be 9.3 and 11.3 (mA/cm^2), fill factor were 0.465 and 0.468 and conversion efficiency (η) 2.08 and 2.5 for eosin-Y sensitized TiO_2 and TiO_2–SiO_2 respectively. Using eosin y sensitized TiO_2 photo anodes Deepa et al., [4] achieved 1.52% PCE, Mali et al., [5] achieved 1.5% PCE and Sarode et al., [22] achieved 1.10% PCE. Our results show the better performance when compare with the previous reports.

The increase in efficiency of TiO_2–SiO_2 based DSSC has two reasons. The first one is porous structure of TiO_2 and TiO_2–SiO_2 film is an important factor to increase the power conversion efficiency. The porous structure is the supporter for adsorbing dye molecules and the diffusion path of electrolyte in the DSSCs was generated after the binder Triton X-100 combusted at 400 °C [15]. These pores could increase the surface area of the TiO_2 and TiO_2–SiO_2 film resulting in the large amount of dye adsorbed on the surface of TiO_2 and TiO_2–SiO_2 films. Meanwhile the pores could increase the contact area between dye molecules and the electrolyte contributing to the oxidized dye being reduced immediately by I_3^- in the electrolyte. The DSSC is rather a complicated system including many processes such as light adsorption, charge injection, charge collection and electrolyte diffusion [23]. The BET analysis shows that doping of SiO_2 in TiO_2 increases the surface area of the composites. Increasing the surface area of the composites increases

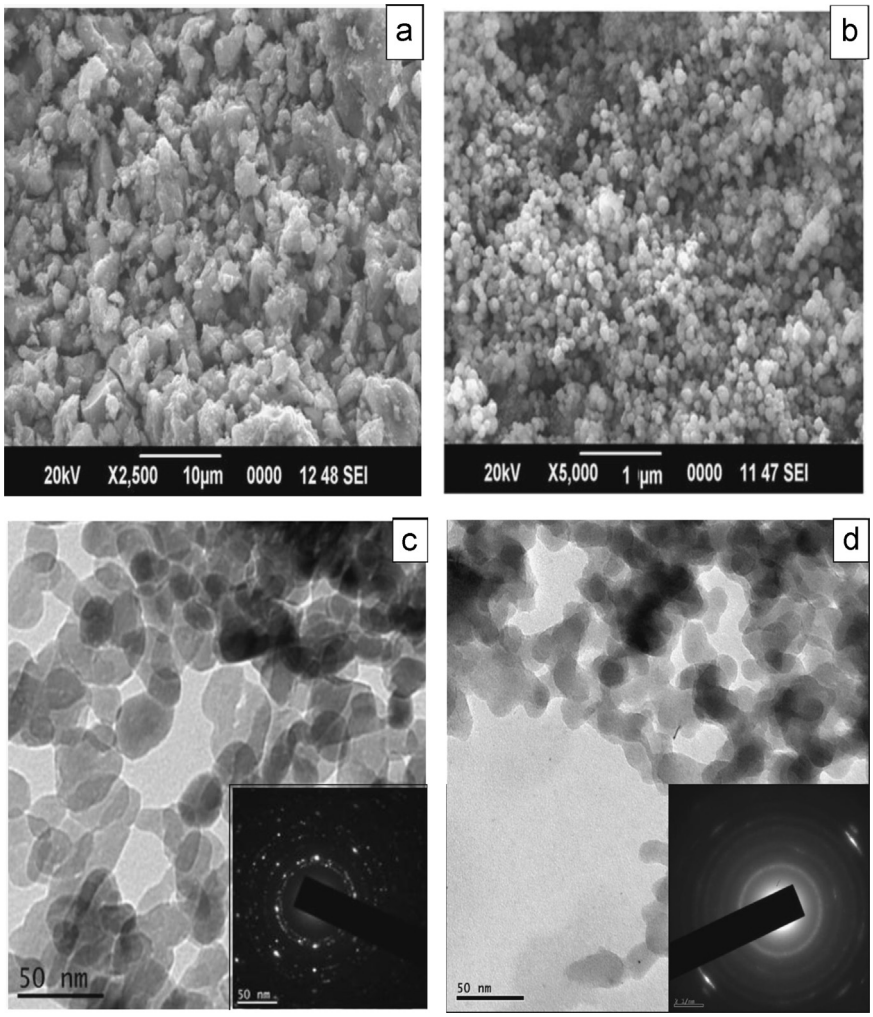


Fig. 4. (a) and (b) SEM and (c) and (d) TEM images of TiO_2 and TiO_2–SiO_2 nanocomposites.

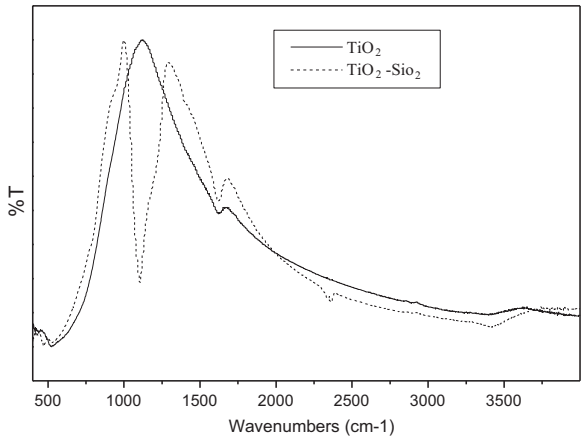


Fig. 5. FTIR spectra of TiO_2 and TiO_2–SiO_2 nanocomposites.

the dye adsorption on the surface. So the TiO_2–SiO_2 shows higher power conversion efficiency when compare with pure TiO_2.

Another one is present study reports the effect of SiO_2 in TiO_2–SiO_2 based DSSC. There are some reports on the formation of energy barrier on semiconductor electrodes by coating a thin layer of insulating oxide such as Al_2O_3, MgO, SiO_2, ZnO, ZrO_2, etc., [24]. Energy barrier at the semiconductor/electrolyte interface was found to decrease the interaction between the photo-excited electrons in the semiconductor electrode and the electrolyte [25]. The suppression of charge recombination has been known due to the tunneling effect [26] that allows electron injection across the barrier (thin insulating oxide layer) and prevents the electron leakage from the semiconductor to the electrolyte. On SiO_2 addition in TiO_2 it becomes positively charged under the optimal experimental conditions (acidic pH). Meanwhile, SiO_2 releases proton (H^+) under the acidic pH value and becomes negatively charged. Consequently, positively charged titania and negatively charged silica attract one another to form a titania–silica complex in the composite. The addition of SiO_2 in TiO_2 increases the number of protons in the composite that was beneficial to the formation of positively charged titania, resulting in maximum current density on TiO_2–SiO_2 composites. The role of SiO_2 as an energy barrier in TiO_2/SiO_2 film is

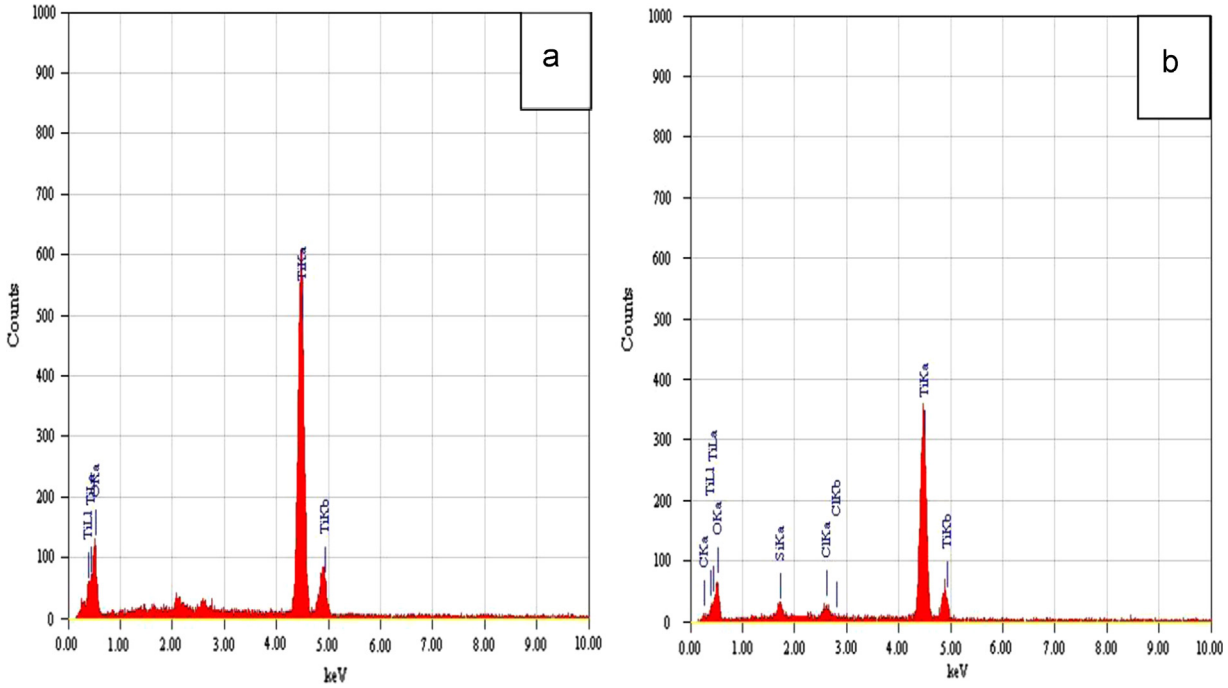


Fig. 6. EDAX analysis of (a) TiO_2 (b) TiO_2–SiO_2 nanocomposites.

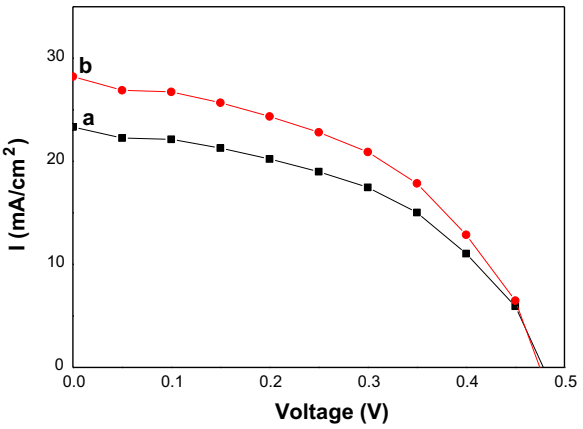


Fig. 7. *I–V* characteristics of (a) TiO_2-eosin-Y, (b) TiO_2–SiO_2-eosin-Y under light illumination.

well consistent and supported by the photovoltaic performance. TiO_2/SiO_2 based DSSCs show superior photovoltaic performance compared to the bare TiO_2 counterparts.

4. Conclusion

TiO_2 and TiO_2–SiO_2 nanocomposites were successfully synthesized by the Sol–gel method and it was characterized by XRD, SEM, TEM, UV–visible, EDAX, FTIR and BET analysis. The synthesized nanoparticles and nanocomposites show good photovoltaic performance in eosin-Y sensitized TiO_2 and TiO_2–SiO_2. When compared with eosin-Y sensitized TiO_2, TiO2–SiO_2 shows 16% higher efficiency. The study reveals that doping of SiO_2 in TiO_2 supress the grain growth, change the morphology, increase the surface area and increase the PCE in DSSC.

Appendix A. Supporting information

Supplementary data associated with this article can be found in the online version at http://dx.doi.org/10.1016/j.mssp.2015.02.071.

References

[1] B. Oregan, M. Gratzel, Nature 353 (1991) 737–740.
[2] A. Hagfeldt, M. Gratzel, Chem. Rev. 95 (1995) 49–68.
[3] S.S. Kanmani, K. Ramachandran, J. Renew. Energy 43 (2012) 149–156.
[4] K.G. Deepa, P. Lekha, S. Sindhu, Sol. Energy 86 (2012) 326–330.
[5] Sawanta S. Mali, C.A. Betty, P.N. Bhosale, P.S. Patil, Electrochim. Acta 59 (2012) 113–120.
[6] J. Yu, J.C. Yu, X. Zhao, J. Sol–Gel Sci. Technol. 24 (2002) 95–103.
[7] X. Meng, Z. Qian, H. Wang, X. Gao, S. Zhang, M. Yang, J. Sol–Gel Sci. Technol. 46 (2008) 195–200.
[8] M. Machida, K. Norimoto, T. Watanabe, K. Hashimoto, A. Fujishima, J. Mater. Sci. 34 (1999) 2569–2574.
[9] L. Zhou, S. Yan, B. Tian, J. Zhang, M. Anpo, Mater. Lett. 60 (2006) 396–399.
[10] A. Ennaoui, B.R. Sankapal, V. Skryshevsky, M.C. Lux-Steiner, Sol. Energy Mater. Sol. Cells 90 (2006) 1533–1541.
[11] P. Cheng, M. Zheng, Y. Jin, Q. Huang, M. Gu, Mater. Lett. 57 (2003) 2989–2994.
[12] Zhai Jiwei, Zhang Liangying, Yao Xi, S.N.B. Hodgson, Surf. Coat. Technol. 138 (2001) 135–140.
[13] U.G. Akpan, B.H. Hameed, Appl. Catal. A: Gen. 375 (2010) 1–11.
[14] Espen Olsen, Georg Hagen, Sten Eric Lindquist, Sol. Energy Mater. Sol. Cells 63 (2000) 267–273.

[15] Yan-Shuang Wei, Qian-Qian Jin, Tie-Zhen Ren, Solid-State Electron. 63 (2011) 76–82.
[16] Jung Gyu Nam, Young Jun Park, Bum Sung Kim, Jai Sung Lee, Scr. Mater. 62 (2010) 148–150.
[17] Takurou N. Murakami, Seigo Ito, Qing Wang, Md. Khaja Nazeeruddin, Takeru Bessho, Ilkay Cesar, Paul Liska, Robin Humphry-Baker, Pascal Comte, Peter Pechy, Michael Grätzel, J. Electrochem. Soc. 153 (2006) 2255–2261.
[18] Kiyoaki Imoto, Kohshin Takahashi, Takahiro Yamaguchi, Teruhisa Komura, Jun-ichi Nakamura, Kazuhiko Murata, Sol. Energy Mater. Sol. Cells 79 (2003) 459–469.
[19] P.K. Khanna, Narendra Singh, Shobhit Charan, Mater. Lett. 61 (2007) 4725–4730.
[20] K. Balachandran, Rajendran Venckatesh, Rajeshwari Sivaraj, P. Rajiv, Spectrochim. Acta A: Mol. Biomol. Spectrosc. 128 (2014) 468–474.
[21] S. Monticone, R. Tufeu, A.V. Kanaev, E. Scolan, C. Sanchez, Appl. Surf. Sci. 162 (2000) 565–570.
[22] M.T. Sarode, Y.B. Khollam, S.R. Jadkar, B.B. Kale, K.C. Mohite, Sol. Energy 106 (2014) 48–55. August.
[23] J.T. Jiu, F.M. Wang, M. Sakamoto, J. Takao, M. Adachi, Sol. Energy Mater. Sol. Cells 87 (2005) 77–80.
[24] Y. Diamant, S.G. Chen, O. Melamed, A. Zaban, J. Phys. Chem. B 107 (2003) 1977–1981.
[25] E. Palomares, J.N. Clifford, S.A. Haque, T. Lutz, J.R. Durrant, J. Am. Chem. Soc. 125 (2003) 475–482.
[26] K. Tennakone, P.K.M. Bandaranayake, P.V.V. Jayaweera, A. Konno, G.R.R.A. Kumara, Physica E 14 (2002) 190–196.